

## Kibble-Zurek mechanism for nonequilibrium phase transitions in driven systems with quenched disorder

C. J. O. Reichhardt<sup>1</sup>  <sup>✉</sup>, A. del Campo<sup>2,3</sup>  & C. Reichhardt<sup>1</sup>

We show that the Kibble-Zurek mechanism applies to nonequilibrium phase transitions found in driven assemblies of superconducting vortices and colloids moving over quenched disorder where a transition occurs from a plastic disordered flowing state to a moving anisotropic crystal. We measure the density of topological defects as a function of quench rate through the nonequilibrium phase transition, and find that on the ordered side of the transition, the topological defect density  $\rho_d$  scales as a power law,  $\rho_d \propto 1/t_q^\beta$ , where  $t_q$  is the quench time duration, consistent with the Kibble-Zurek mechanism. We show that scaling with the same exponent holds for varied strengths of quenched disorder and that the exponents fall in the directed percolation universality class. Our results suggest that the Kibble-Zurek mechanism can be applied to the broader class of systems that exhibit absorbing phase transitions.

<sup>1</sup>Theoretical Division and Center for Nonlinear Studies, Los Alamos National Laboratory, Los Alamos, NM 87545, USA. <sup>2</sup>Department of Physics and Materials Science, University of Luxembourg, L-1511 Luxembourg, Luxembourg. <sup>3</sup>Donostia International Physics Center, E-20018 San Sebastián, Spain. <sup>✉</sup>email: [cjrx@lanl.gov](mailto:cjrx@lanl.gov)

In systems that exhibit second-order phase transitions, a disordered phase on one side of the transition, such as a liquid or glass state, can be characterized by the presence of topological defects, while on the other side of the transition, there is an ordered or defect-free state such as a crystal. The defect-free ordered phase arises when the parameter controlling the transition is changed very slowly so that the system remains within the adiabatic limit. If the rate of change through the transition increases, a portion of the topological defects do not have time to annihilate, and persist on the ordered side of the transition. A scenario for understanding the behavior for varied quench rates across a continuous phase transition is the Kibble–Zurek (KZ) mechanism, which predicts a universal power law for the defect density  $\rho_d \propto t_q^{-\beta}$ , where  $t_q$  is the time duration of the quench through the transition, so that slower quenches produce fewer defects<sup>1–4</sup>. The KZ mechanism has been studied in a variety of systems at the transition into an ordered phase, where the scaling exponents can be related to the universality class of the underlying phase transition<sup>5–11</sup>.

The KZ scenario has generally been applied to systems that have equilibrium phase transitions; however, there have been recent proposals to use the KZ scenario to address transitions between different nonequilibrium steady states<sup>12–17</sup>, such as those that occur in optical systems or for Rayleigh–Bénard convection, where defects can arise in otherwise hexagonal ordered lattices. More recently, there has also been work examining KZ scenarios in nonequilibrium quantum systems<sup>18–20</sup> including dissipative systems<sup>19</sup>. In these works, the transitions were of the Berezinskii–Kosterlitz–Thouless type, which also appears in equilibrium systems; however, these works indicate that the KZ scenario can be applied more broadly to nonequilibrium systems.

Another class of nonequilibrium systems consists of assemblies of particles driven over quenched disorder that exhibit behavior consistent with a continuous phase transition from a disordered state to an ordered state<sup>21–25</sup> or from a dynamical fluctuating state to a non-fluctuating state<sup>26–29</sup>. This phenomenon is often described in terms of an absorbing phase transition in the directed percolation (DP) class, which is observed in a wide range of nonequilibrium systems<sup>26</sup>. The DP transition is particularly interesting since it is an example of a pure nonequilibrium transition that cannot occur in an equilibrium system. If the KZ scenario could be observed in a system with a DP or absorbing phase transition, this would pave the way to applying the KZ analysis to an entirely new class of nonequilibrium systems. Such systems have several features that make them ideal for studying the KZ scenario. They often contain very well-defined topological defects, and the transition can occur at  $T=0$ , so thermal effects such as critical coarsening on the ordered side of the transition are absent and very large systems are experimentally accessible.

One of the best examples of a system that shows evidence for a continuous nonequilibrium phase transition as a function of a continuously changing driving parameter from a disordered fluctuating state with a high density of topological defects to a dynamically ordered non-fluctuating state in which topological defects are scarce or absent is superconducting vortices driven over quenched disorder<sup>21,22,30–41</sup>. At  $T=0$  and in the absence of quenched disorder, a superconducting vortex system forms a triangular lattice-free of defects; however, when the quenched disorder is present, a disordered state containing numerous topological defects can appear that can be characterized as a vortex glass<sup>42</sup>. A finite external drive in the form of an applied current causes vortices in the disordered state to depin and move<sup>24,42</sup>. For drives above depinning, the system enters a strongly fluctuating or plastically flowing state in which there is a fluctuating number of topological defects, while at higher drives,

there is a critical driving force above which the vortices dynamically order into a state with zero or a small number of topological defects<sup>22,24,32–37</sup>. This ordered state is not isotropic but takes the form of a moving anisotropic crystal<sup>24,33,34,36,37</sup> or a moving smectic state<sup>32,34–38</sup>. Here, a small number of topological defects in the form of dislocations are present which have their Burgers vectors aligned in the direction of the drive. The critical drive amplitude at which the ordering transition occurs is a function of vortex density and disorder strength<sup>24</sup>. The ordering transition has been observed experimentally by direct imaging<sup>36,39</sup>, neutron scattering<sup>30</sup>, changes in the noise<sup>37,38,41</sup>, and changes in transport curve features<sup>21,24,31–33,37,40</sup>. This same type of dynamical ordering transition is general to the broader class of particle-like assemblies driven over quenched disorder, and it has been studied for colloidal particles moving over disordered landscapes<sup>23,24,43–45</sup>, moving Wigner crystals<sup>46</sup>, sliding charged systems<sup>47</sup>, driven pattern forming states<sup>48,49</sup>, driven dislocations<sup>50</sup>, and magnetic skyrmions moving over quenched disorder<sup>51</sup>. Since the transition from the disordered state to the ordered state is controlled by changing the driving amplitude, the number of topological defects on the ordered side of the transition can be measured for varied drive sweep rates across the transition to test the predictions of the KZ scenario.

Here we explore the question of whether the KZ scenario is obeyed for nonequilibrium phase transitions in driven systems with a quenched disorder for varied sweep rates through the transition. We numerically examine the density of defects in driven vortex and colloidal systems at  $T=0$  for varied driving sweep rates through the dynamical ordering transition. We find that the defect density obeys  $\rho_d \propto t_q^{-\beta}$ , where  $t_q$  is the time required to go through the transition, consistent with the KZ scenario. The same behavior appears for various values of the quenched disorder and for both vortices and colloids moving over a random substrate. The exponent we find in both systems is  $\beta \approx 0.39$ , consistent with an underlying transition that falls in a directed percolation (DP) universality class, which often describes nonequilibrium phase transitions from fluctuating states to non-fluctuating states<sup>26,27,29</sup>. These results could be tested experimentally in superconducting vortex systems, colloids, or other driven systems with quenched disorder. Our results also imply that the KZ mechanism could be applied generally to nonequilibrium phase transitions in the same way that it has been applied to equilibrium phase transitions, and that it could be tested in many other types of driven systems that show dynamical continuous transitions from disordered to ordered states.

## Results

**Modeling and characterization of the nonequilibrium phase transition.** We use a well-established simulation model for superconducting vortices driven over random disorder. The vortices are represented as repulsively interacting point particles which undergo a dynamical ordering transition from a disordered plastic flow phase to a moving ordered crystal or smectic state<sup>22,24,32,33,37,38</sup>. We consider a two-dimensional (2D) system of size  $L \times L$ , with  $L = 36\lambda$  in units of the London penetration depth, containing a fixed number  $N$  of vortices produced by an external magnetic field  $\mathbf{B} = B\hat{z}$ . The vortex density is  $n_v = N/L^2$ . The motion of vortex  $i$  at position  $\mathbf{R}_i$  is obtained by integrating the overdamped equation of motion

$$\eta \frac{d\mathbf{R}_i}{dt} = \mathbf{F}_{vv} + \mathbf{F}_i^{pp} + \mathbf{F}_d, \quad (1)$$

where the damping constant  $\eta = 1.0$ . The vortex–vortex interaction force  $\mathbf{F}_i^{vv} = \sum_{j=1}^N f_0 K_1(R_{ij}/\lambda) \hat{\mathbf{R}}_{ij}$ , where  $K_1$  is the modified Bessel function,  $R_{ij} = |\mathbf{R}_i - \mathbf{R}_j|$  is the distance between vortex  $i$

and  $j$ ,  $\hat{\mathbf{R}}_{ij} = (\mathbf{R}_i - \mathbf{R}_j)/R_{ij}$ ,  $f_0 = \phi_0^2/2\pi\mu_0\lambda^3$ ,  $\mu_0$  is the permeability of free space, and  $\phi_0 = h/2e$  is the elementary flux quantum. The modified Bessel function  $K_1$  falls off exponentially for  $R_{ij}/\lambda > 1.0$ . The vortices are confined to the  $x, y$  plane and the magnetic field is applied in the  $z$ -direction. The quenched disorder is modeled by  $N_p$  randomly placed harmonically attractive pinning sites of radius  $r_p$  with  $\mathbf{F}_i^{\text{pp}} = -\sum_{k=1}^{N_p} (F_p/r_p)(\mathbf{R}_i - \mathbf{R}_k^{(p)})\Theta(r_p - |\mathbf{R}_i - \mathbf{R}_k^{(p)}|)\hat{\mathbf{R}}_{ik}^{(p)}$  where  $F_p$  is the maximum pinning force,  $\mathbf{R}_k^{(p)}$  is the location of pinning site  $k$ , and  $\hat{\mathbf{R}}_{ik}^{(p)} = (\mathbf{R}_i - \mathbf{R}_k^{(p)})/|\mathbf{R}_i - \mathbf{R}_k^{(p)}|$ . The pinning density is  $n_p = N_p/L^2$ . The driving force  $\mathbf{F}_d$  is applied uniformly to all the vortices, and corresponds experimentally to a Lorentz force  $\mathbf{F}_d = \mathbf{B} \times \mathbf{J} = F_D f_0 \hat{\mathbf{x}}$ , where  $\mathbf{J}$  is the applied current. The initial vortex configurations are obtained using simulated annealing. We increase the magnitude of the dimensionless driving force from  $F_D = 0$  to a final maximum value over a total time of  $t_q$  in increments of  $\Delta F_D = 0.002$ . Time is reported in dimensionless units achieved by scaling time by  $\tau = \eta/f_0$ . We characterize the system by measuring the average velocity per vortex in the driving direction,  $\langle V \rangle = N^{-1} \sum_i \mathbf{v}_i \cdot \hat{\mathbf{x}}$ , and the fraction of sixfold coordinated vortices,  $P_6 = N^{-1} \sum_i \delta(z_i - 6)$ , where  $z_i$  is the coordination number of vortex  $i$  obtained from a Voronoi construction. We also compute the fraction of topological defects  $P_D = 1 - P_6$ .

**Numerical results.** Figure 1 illustrates the effect of changing  $F_D$  in the adiabatic limit for a system with  $n_v = 1.0$ ,  $n_p = 0.5$ ,  $F_p = 0.4$ , and  $r_p = 0.3$ . In Fig. 1a we plot the average vortex velocity  $\langle V \rangle$

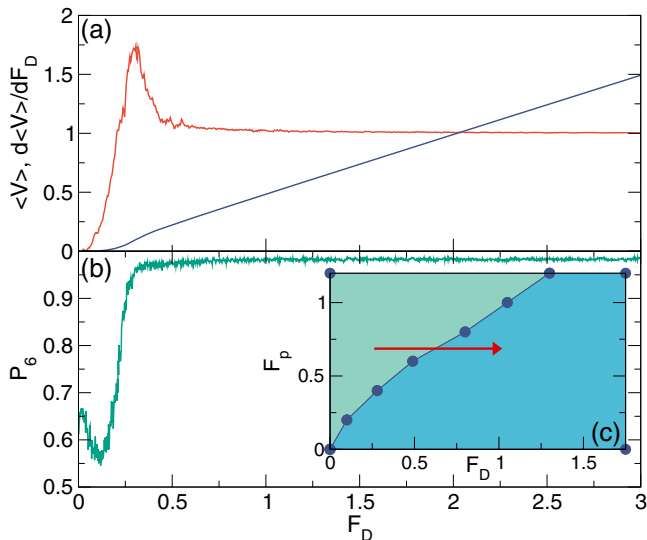


**Fig. 1 Dynamical phase transition in a superconducting vortex system.**

**a** The velocity  $\langle V \rangle$  versus applied drive  $F_D$  (blue) and the corresponding  $d\langle V \rangle/dF_D$  vs  $F_D$  (red) for a 2D superconducting vortex system with quenched disorder at vortex density  $n_v = 1.0$ , pinning density  $n_p = 0.5$ , pinning force  $F_p = 0.4$ , and pinning radius  $r_p = 0.3$ . The curves are from a single simulation and are obtained for a quenching time of  $t_q = 7.5 \times 10^6$ , which is considered the adiabatic limit. **b** The corresponding fraction of sixfold coordinated vortices  $P_6$  vs  $F_D$ . A nonequilibrium transition from a disordered state to an ordered state occurs for  $F_D \approx 0.3$ . **c** Dynamical phase diagram as a function of  $F_p$  versus  $F_D$  for the same system highlighting the disordered phase (green) and the dynamically ordered phase (blue). The arrow indicates the direction in which the transition is crossed at different sweep rates. The error bars representing the uncertainty in the location of the depinning transition, obtained from multiple realizations, are smaller than the symbols.

along with  $d\langle V \rangle/dF_D$  versus  $F_D$  for  $t_q = 7.5 \times 10^6$ . If  $t_q$  is increased to a larger value, the curves remain nearly unchanged. Figure 1b shows the corresponding fraction of sixfold coordinated vortices  $P_6$  versus  $F_D$ , where we would have  $P_6 = 1$  for a triangular lattice. A depinning transition occurs near  $F_D = 0.06$ , and for  $F_D < 0.225$  we find  $P_6 \approx 0.64$ , indicating a highly defected or disordered state in which the vortices are undergoing plastic flow. In Fig. 2a we show a Voronoi plot of a snapshot of the vortex positions from the system in Fig. 1 at  $F_D = 0.1$ , where numerous dislocations are present. As Fig. 1b indicates, for  $F_D > 0.4$  there is a regime in which  $P_6$  increases until it reaches the value  $P_6 = 0.98$ , where the vortices form an anisotropic triangular lattice of the type shown in Fig. 2b at  $F_D = 1.5$  in the ordered state. Here the lattice is aligned in the driving direction and contains a small number of aligned dislocations, forming a smectic state as studied previously<sup>32–34,36,37</sup>. The critical force for the transition from the disordered state to the dynamically ordered phase is  $F_D^c \approx 0.3$ . We do not observe any hysteresis across the transition, which has features consistent with a second-order transition. In Fig. 1a, there is a peak in  $d\langle V \rangle/dF_D$  in the plastic flow phase near  $F_D = 0.15$  followed by a saturation near  $F_D = 0.3$  to  $d\langle V \rangle/dF_D \approx 1.0$ , in agreement with previous studies of the dynamical ordering transition<sup>21,31,33,38,40,41</sup>. The critical driving force for dynamic ordering also depends on the strength of the disorder, as shown in Fig. 1c where we plot a dynamical phase diagram for the system in Fig. 1a, b as a function of  $F_p$  versus  $F_D$  at  $t_q = 7.5 \times 10^6$ . The disordered and ordered phases are highlighted, and the arrow illustrates the direction in which we sweep across the transition at different rates.

Now that we have established the driving force which separates the disordered and ordered phases, we can cross this transition for varied  $t_q$ . In Fig. 3a we plot  $P_6$  versus  $F_D$  for the system in Fig. 1 at  $t_q = 7.5 \times 10^6$ ,  $3 \times 10^6$ ,  $7.5 \times 10^5$ ,  $3 \times 10^5$ ,  $7.5 \times 10^4$ ,  $3 \times 10^4$ ,  $7.5 \times 10^3$ ,  $3 \times 10^3$ , and 750, showing that as the quench rate increases and  $t_q$  becomes smaller, the fraction of sixfold coordinated particles on the ordered side of the critical transition value  $F_D^c = 0.3$  drops. The final defect density as a function of  $t_q$  appears in Fig. 3b, c.

We illustrate Voronoi plots of the final  $F_D = 1.5$  state for the system in Fig. 3 at  $t_q = 7.5 \times 10^3$  in Fig. 4(a),  $t_q = 3 \times 10^4$  in Fig. 4b,  $t_q = 7.5 \times 10^4$  in Fig. 4c, and  $t_q = 3 \times 10^5$  in Fig. 4d, indicating that the number of remaining defects is larger for

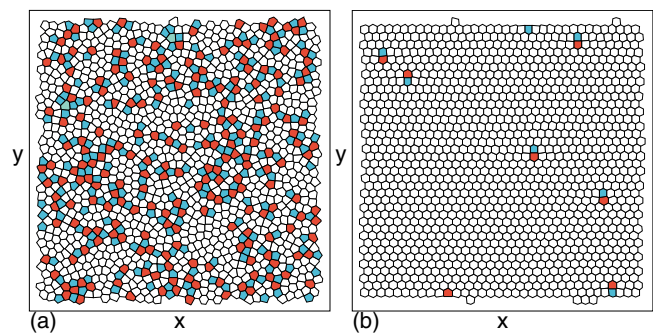


**Fig. 2 Vortex configurations on either side of the dynamical phase transition.** Voronoi constructions of snapshots of the vortex positions in the system from Fig. 1 with vortex density  $n_v = 1.0$ , pinning density  $n_p = 0.5$ , pinning force  $F_p = 0.4$ , pinning radius  $r_p = 0.3$ , and quench time  $t_q = 7.5 \times 10^6$ . White polygons are sixfold coordinated, red polygons are sevenfold coordinated, and blue polygons are fivefold coordinated. **a** A driving force of  $F_D = 0.1$  in the disordered phase with numerous defects. **(b)**  $F_D = 1.5$  in the dynamically ordered phase. The vortex lattice is aligned in the driving direction and there is a small number of aligned dislocations.

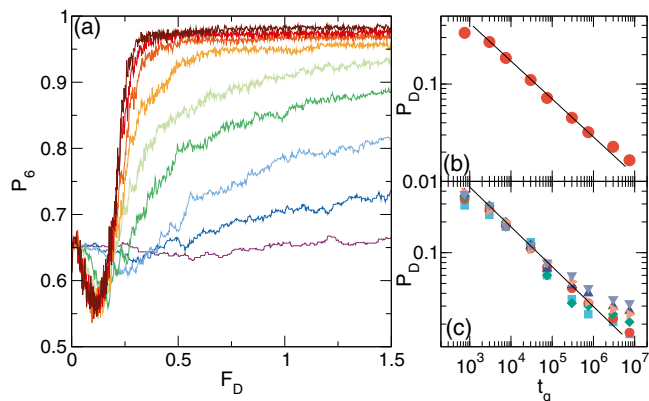


**Fig. 3 Transition from the disordered to the ordered state for superconducting vortices as a function of quenching speed.** **a** The fraction of sixfold coordinated vortices  $P_6$  versus driving force  $F_D$  for the system in Fig. 1 with vortex density  $n_v = 1.0$ , pinning density  $n_p = 0.5$ , pinning force  $F_p = 0.4$ , and pinning radius  $r_p = 0.3$  at quench times of  $t_q = 7.5 \times 10^6, 3 \times 10^6, 7.5 \times 10^5, 3 \times 10^5, 7.5 \times 10^4, 3 \times 10^4, 7.5 \times 10^3, 3 \times 10^3$ , and 750, from top to bottom. **b** The final defect density  $P_D = 1 - P_6$  at  $F_D = 1.5$  in the same system versus  $t_q$ . The solid line is a power-law fit with exponent  $\beta = -0.385$ . **c**  $P_D$  versus  $t_q$  for the same system at different values of  $F_p = 0.2$  (blue squares),  $0.4$  (red circles),  $0.6$  (green diamonds),  $0.8$  (blue up triangles),  $1.0$  (orange right triangles), and  $1.2$  (purple down triangles). The solid line is a power-law fit with  $\beta = -0.39$ . Error bars in **(b, c)** representing the uncertainty in the defect density, obtained from multiple realizations, are smaller than the data markers.

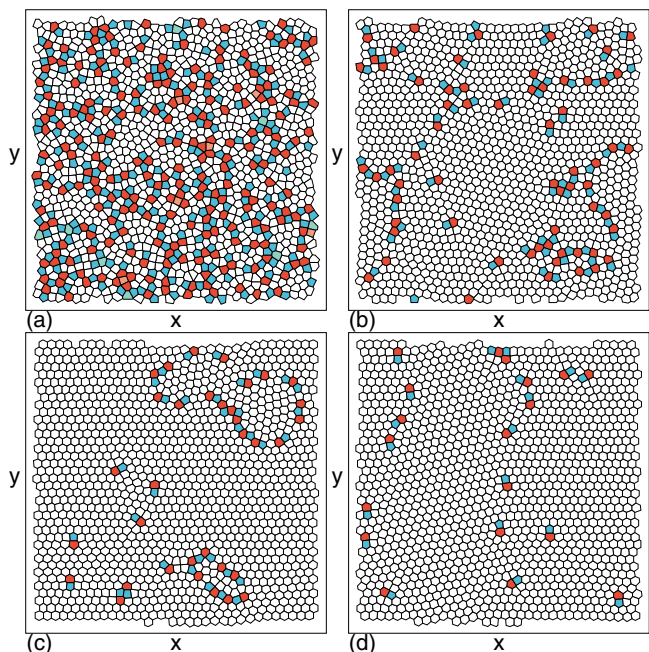


**Fig. 4 Final ordering of lattice at different quenching speeds.** Voronoi plots of the final driving force  $F_D = 1.5$  state for the system in Fig. 3a, b with vortex density  $n_v = 1.0$ , pinning density  $n_p = 0.5$ , pinning force  $F_p = 0.4$ , and pinning radius  $r_p = 0.3$  at quench times of **(a)**  $t_q = 7.5 \times 10^3$ , **(b)**  $3 \times 10^4$ , **(c)**  $7.5 \times 10^4$ , and **(d)**  $3 \times 10^5$ . The number of defects is larger for smaller  $t_q$  or a faster sweep rate.

smaller  $t_q$ . Figure 2b shows the same sample in the adiabatic limit with  $t_q = 7.5 \times 10^6$ . The defects that appear on the ordered side of the transition generally take the form of dislocations composed of pairs of fivefold and sevenfold coordinated particles. At larger  $t_q$ ,

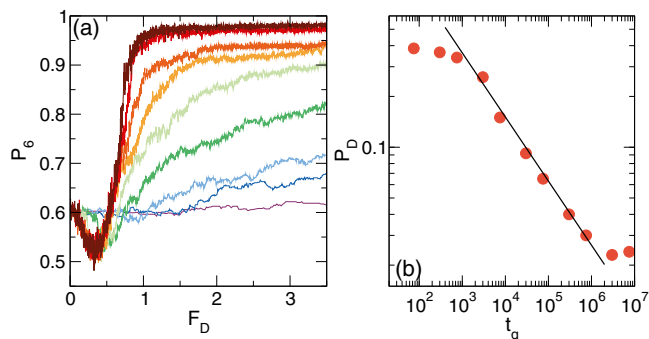


**Fig. 5 Transition from the disordered to the ordered state for colloidal particles as a function of quenching speed.** **a** The fraction of sixfold coordinated colloids  $P_6$  versus driving force  $F_D$  for a colloidal system with colloidal density  $n_c = 1.0$ , pinning density  $n_p = 0.5$ , pinning force  $F_p = 1.0$ , and pinning radius  $r_p = 0.35$  at quench times of  $t_q = 3 \times 10^6, 7.5 \times 10^5, 3.0 \times 10^5, 7.5 \times 10^4, 3.0 \times 10^4, 7.5 \times 10^3, 750, 300$ , and 75, from top to bottom. **b** The defect density  $P_D$  vs  $t_q$  for the system in **(a)** obtained at  $F_D = 2.5$ . The solid line is a power-law fit with exponent  $\beta = -0.39$ . Error bars representing the uncertainty in the defect density, obtained from multiple realizations, are smaller than the data markers.

the dislocations have their Burgers vectors oriented in the direction of drive, giving rise to a smectic ordering in which the system can be regarded as a set of one-dimensional (1D) moving channels. In Fig. 3b we plot  $P_D = 1 - P_6$ , the density of topological defects at the final  $F_D = 1.5$  state on the ordered side of the transition, versus  $t_q$ . We find  $P_D \propto t_q^\beta$ , where the solid line indicates a fit with  $\beta = -0.385$ . The KZ scenario predicts a power-law decay of  $P_D$  with increasing  $t_q$ . If we choose a final value of  $F_D$  which is closer to but still above the critical transition drive  $F_c$ , the scaling is not as good at smaller  $t_q$  but we still find the same exponent for the larger values of  $t_q$ .

The plots of  $P_D$  versus  $t_q$  in Fig 3c indicate that the same scaling behavior remains robust over a range of different values of  $F_p$  from  $F_p = 0.2$  to  $F_p = 1.2$ . Since  $F_c$  varies with  $F_p$ , for each sample we select a final value of  $F_D$  that is the same distance above  $F_c$  for consistency. The straight line is a power-law fit with  $\beta = 0.39$ . For large  $F_p$ , the scaling at larger values of  $t_q$  is not as good because more defects become trapped by the pinning.

In addition to superconducting vortices, we have also considered colloidal particles driven over quenched disorder. Here we use the same type of overdamped simulations but replace the particle-particle interactions with the Yukawa or screened Coulomb potential  $U(r_{ij}) = A \exp(-\kappa r_{ij})/r_{ij}^{52}$ , with  $\kappa = 1.0$  and  $A = 0.1$ . The colloidal particles experience a stronger short-range repulsion than the vortices. In experiments, various types of random quenched disorder can be introduced along with an external driving force<sup>45,53</sup>, and the number of topological defects can be measured with imaging techniques<sup>53,54</sup>. In Fig. 5a we show  $P_6$  versus  $F_D$  in a colloidal system with colloidal density  $n_c = 1.0$ ,  $n_p = 0.5$ ,  $F_p = 1.0$ , and  $r_p = 0.35$  at  $t_q = 3 \times 10^6, 7.5 \times 10^5, 3.0 \times 10^5, 7.5 \times 10^4, 3.0 \times 10^4, 7.5 \times 10^3, 750, 300$ , and 75, where the final  $P_6$  decreases for smaller  $t_q$ . In Fig. 5b we plot the final value of  $P_D$  at  $F_D = 2.5$  versus  $t_q$  for the system in Fig. 5a. The solid line is a power-law fit with  $\beta = -0.39$ , similar to the exponent obtained for the vortex case.

**Discussion**

We can ask whether the scaling exponent we obtain can be related to possible universality classes of the dynamical transition. In the KZ scenario, the scaling exponent obeys  $\beta = (D - d)v/(1 + zv)$ , where  $v$  and  $z$  are critical exponents associated with the universality class of the underlying phase transition,  $D$  is the spatial

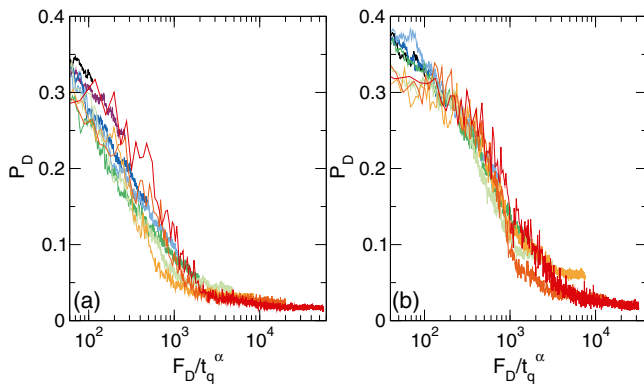


**Fig. 6** Defect density scaling in the vortex and colloid systems.

Dimensionless scaling plots of the defect density  $P_D$  versus the scaled driving force  $F_D/t_q^\alpha$ , where  $t_q$  is the quench time and where the exponent  $\alpha = 0.625$ . **a** The vortex system from Fig. 3a. **b** The colloid system from Fig. 5a.

dimension of the system, and  $d$  is the dimension of the defect. For a 2D Ising model with  $D = 2$ ,  $\beta = 2/3$ , which is not what we observe; however, since the defects in our sample are all aligned in the driving direction, our system is closer to coupled 1D channels, which would give  $\beta = 1/3$ . Recent simulations of certain quenched 2D spin ice models give  $\beta = 0.31^{55}$ . A more likely candidate for the universality class of a nonequilibrium system is directed percolation (DP)<sup>26</sup>, where the critical exponents depend on the effective dimension of the dynamics. If we assume dynamics of dimension  $1 + 1$ , we would have  $z = 1.58$  and  $\nu = 1.097^{26}$ , giving  $\beta = 0.401$ , which is in agreement with the values we observe. We argue that the  $1 + 1$  dynamics may be relevant since the topological defects are mostly aligned in a single direction on the ordered side of the transition, and the relevant length scale could be the distance between the defects in the direction of the drive rather than perpendicular to the drive.

In the KZ scenario, the lag time between the nonequilibrium and equilibrium value is given by the freeze-out time  $\hat{t} \propto (t_q^{z\nu})^{1/(1+z\nu)}$ . Since the value of the driving force  $F_D$  is a function of time, and since  $F_D$  and  $t_q$  are dimensionless, this implies that the defect fraction should scale as  $P_D \propto F_D/t_q^\alpha$ , where  $t_q$  is the quench time. In Fig. 6a we illustrate this scaling for the vortex system from Fig. 3a and in Fig. 6b we show the scaling for the colloidal system from Fig. 5a. In each case, the scaling exponent is  $\alpha = 0.625$ . The KZ prediction gives  $z\nu/(1+z\nu) = \alpha$ , where plugging in the scaling exponents for  $1 + 1$  directed percolation<sup>26</sup> leads to  $\alpha = 0.632$ , consistent with the exponents we find.

To better understand why the dynamics is  $1 + 1$  dimensional, in Fig. 7a we illustrate the colloidal positions and trajectories on the disordered side of the transition for a subset of the system in Fig. 5 at  $F_D = 0.25$  and  $t_q = 7.5 \times 10^5$ , showing strongly disordered flow occurring in both the  $x$  and  $y$  directions. The corresponding Voronoi plot in Fig. 7b contains a high defect density, similar to what is observed in the vortex system in the disordered phase. Figure 7c shows the positions and trajectories of the colloids on the ordered side of the transition at  $F_D = 1.5$ . Here the dynamics are strictly 1D in character, and the topological defects are all aligned in the direction of the drive as shown in Fig. 7d. In theoretical work for particles moving over random disorder in 2D, it is argued that the strongly driven case can be considered as a series of coupled 1D channels that slide past one another to form a moving smectic state<sup>34,35</sup>. This 1D channeling could explain why the dynamics produce scaling exponents consistent with  $1 + 1$  DP rather than  $2 + 1$  DP.

As indicated in the introduction, the KZ scenario has previously been demonstrated in nonequilibrium systems<sup>18–20</sup>;

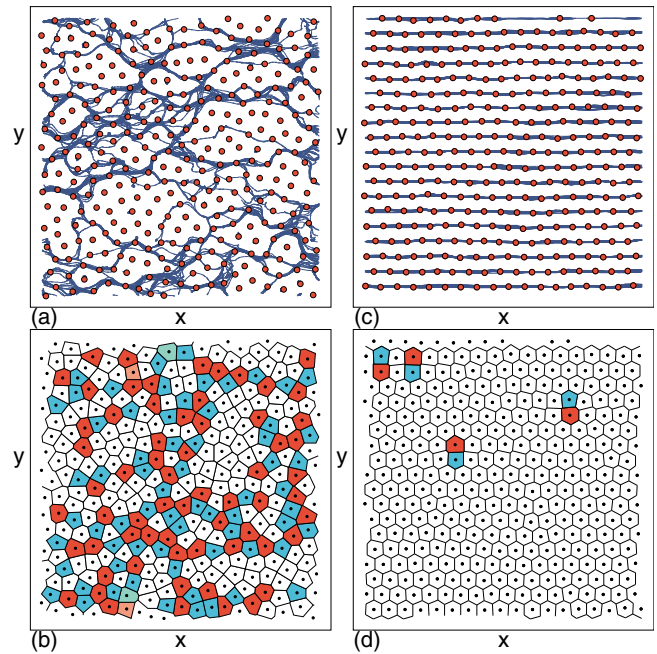


**Fig. 7** Disordered and  $1 + 1$  dimensional flow below and above the dynamical phase transition. **a** The colloid positions (red circles) and trajectories (lines) for a subset of the system in Fig. 5 with colloid density  $n_c = 1.0$ , pinning density  $n_p = 0.5$ , pinning force  $F_p = 1.0$ , and pinning radius  $r_p = 0.35$  at a quench time of  $t_q = 7.5 \times 10^5$  and a driving force of  $F_D = 0.25$ , showing 2D disordered flow. **b** The corresponding Voronoi plot showing a high defect density. **c** The colloid positions and trajectories in the same system at  $F_D = 1.5$  showing 1D channeling. **d** The corresponding Voronoi plot shows that all of the topological defects are aligned in the same direction.

however, these systems are of a different type than the driven particles over the quenched disorder that we consider, and the transitions are versions of equilibrium phase transitions such as the Berezinskii–Kosterlitz–Thouless transition. In our system, the transition is an absorbing phase transition in the directed percolation class<sup>26–29</sup>, which has no equilibrium analog, so our results open the possibility of applying the KZ scenario to a new class of nonequilibrium phase transitions of DP type. In the past, directed percolation systems were very difficult to characterize, and experiments providing strong evidence for the DP transition were first achieved relatively recently<sup>27,28</sup>. Our work suggests that the KZ scenario can be used as a valuable way to characterize systems with absorbing phase transitions. Additionally, since very large-scale experiments can be performed for driven particles over quenched disorder, extensive KZ scaling regimes could be accessed in these systems. Other directions include studying the statistics of the defect distribution<sup>56</sup> or considering very slow annealing<sup>57</sup>.

In conclusion, we have investigated the evolution of the density of defects across a dynamical disorder to order nonequilibrium phase transition for driven particles moving over quenched disorder as we vary the quench rate. We find that the defect density scales as a power law with quench rate, in agreement with the predictions of the Kibble–Zurek scenario. For both superconducting vortices and colloidal assemblies, we find a scaling exponent of  $\beta \approx -0.39$ , which is consistent with an underlying transition that falls in the  $1 + 1$  directed percolation universality class since the ordered system forms a moving smectic state in which the defects are aligned in 1D chains. Experimentally, our predictions could be tested in superconducting vortex systems using various imaging and transport measures that have

previously been shown to be correlated with the number of defects in the vortex lattice<sup>31</sup>. Direct imaging of the dynamics is feasible using colloidal systems, and it would also be possible to consider ac drives which would avoid edge effects. Our results suggest that the Kibble–Zurek scenario can be applied to more general nonequilibrium continuous absorbing phase transitions, particularly those between disordered strongly fluctuating states and ordered weakly fluctuating or non-fluctuating states. Our results also imply that a system undergoing a directed percolation transition could exhibit features of the Kibble–Zurek scenario provided that some type of well-defined defect structure can be identified.

### Data availability

The datasets generated during and/or analyzed during the current study are available from the corresponding author upon reasonable request.

### Code availability

The codes generated and used during the current study are available from the corresponding author on reasonable request.

Received: 4 March 2022; Accepted: 20 June 2022;

Published online: 04 July 2022

### References

- Kibble, T. W. B. Topology of cosmic domains and strings. *J. Phys. A Math. Gen.* **9**, 1387–1398 (1976).
- Zurek, W. H. Cosmological experiments in superfluid-helium. *Nature* **317**, 505–508 (1985).
- Zurek, W. H. Cosmological experiments in condensed matter systems. *Phys. Rep.* **276**, 177 (1996).
- del Campo, A. & Zurek, W. H. Universality of phase transition dynamics: Topological defects from symmetry breaking. *Int. J. Mod. Phys. A* **29**, 1430018 (2014).
- Bowick, M. J., Chandar, L., Schiff, E. A. & Srivastava, A. M. The cosmological Kibble mechanism in the laboratory: string formation in liquid crystals. *Science* **263**, 943–945 (1994).
- Weiler, C. N. et al. Spontaneous vortices in the formation of Bose-Einstein condensates. *Nature* **455**, 948 (2008).
- Ulm, S. et al. Observation of the Kibble-Zurek scaling law for defect formation in ion crystals. *Nat. Commun.* **4**, 2290 (2013).
- Pyka, K. et al. Topological defect formation and spontaneous symmetry breaking in ion Coulomb crystals. *Nat. Commun.* **4**, 2291 (2013).
- Deuschländer, S., Dillmann, P., Maret, G. & Keim, P. Kibble-Zurek mechanism in colloidal monolayers. *Proc. Natl Acad. Sci. USA* **112**, 6925 (2015).
- Keesling, A. et al. Quantum Kibble-Zurek mechanism and critical dynamics on a programmable Rydberg simulator. *Nature* **568**, 207 (2019).
- Ko, B., Park, J. W. & Shin, Y. Kibble-Zurek universality in a strongly interacting Fermi superfluid. *Nat. Phys.* **15**, 1227 (2019).
- Ducci, S., Ramazza, P. L., González-Viñas, W. & Arecchi, F. T. Order parameter fragmentation after a symmetry-breaking transition. *Phys. Rev. Lett.* **83**, 5210–5213 (1999).
- Casado, S., González-Viñas, W., Mancini, H. & Boccaletti, S. Topological defects after a quench in a Bénard-Marangoni convection system. *Phys. Rev. E* **63**, 057301 (2001).
- Casado, S., González-Viñas, W. & Mancini, H. Testing the Kibble-Zurek mechanism in Rayleigh-Bénard convection. *Phys. Rev. E* **74**, 047101 (2006).
- Casado, S., González-Viñas, W., Boccaletti, S., Ramazza, P. L. & Mancini, H. The birth of defects in pattern formation: testing of the Kibble-Zurek mechanism. *Eur. Phys. J. Spec. Top.* **146**, 87–98 (2007).
- Miranda, M. A., Burguete, J., González-Viñas, W. & Mancini, H. Exploring the Kibble-Zurek mechanism in a secondary bifurcation. *Int. J. Bifurc. Chaos* **22**, 1250165 (2012).
- Miranda, M. A., Burguete, J., Mancini, H. & González-Viñas, W. Frozen dynamics and synchronization through a secondary symmetry-breaking bifurcation. *Phys. Rev. E* **87**, 032902 (2013).
- Dziarmaga, J. & Zurek, W. H. Quench in the 1D Bose-Hubbard model: topological defects and excitations from the Kosterlitz-Thouless phase transition dynamics. *Sci. Rep.* **4**, 5950 (2014).
- Zamora, A. et al. Kibble-Zurek mechanism in driven dissipative systems crossing a nonequilibrium phase transition. *Phys. Rev. Lett.* **125**, 095301 (2020).
- Schmitt, M., Rams, M. M., Dziarmaga, J., Heyl, M. & Zurek, W. H. Quantum phase transition dynamics in the two-dimensional transverse-field Ising model. Preprint at arXiv <https://arxiv.org/abs/2106.09046> (2021).
- Bhattacharya, S. & Higgins, M. J. Dynamics of a disordered flux line lattice. *Phys. Rev. Lett.* **70**, 2617–2620 (1993).
- Koshelev, A. E. & Vinokur, V. M. Dynamic melting of the vortex lattice. *Phys. Rev. Lett.* **73**, 3580–3583 (1994).
- Bohlein, T. & Bechinger, C. Experimental observation of directional locking and dynamical ordering of colloidal monolayers driven across quasiperiodic substrates. *Phys. Rev. Lett.* **109**, 058301 (2012).
- Reichhardt, C. & Reichhardt, C. J. O. Depinning and nonequilibrium dynamic phases of particle assemblies driven over random and ordered substrates: a review. *Rep. Prog. Phys.* **80**, 026501 (2017).
- Sándor, C., Libál, A., Reichhardt, C. & Olson Reichhardt, C. J. Dynamic phases of active matter systems with quenched disorder. *Phys. Rev. E* **95**, 032606 (2017).
- Hinrichsen, H. Non-equilibrium critical phenomena and phase transitions into absorbing states. *Adv. Phys.* **49**, 815–958 (2000).
- Takeuchi, K. A., Kuroda, M., Chaté, H. & Sano, M. Directed percolation criticality in turbulent liquid crystals. *Phys. Rev. Lett.* **99**, 234503 (2007).
- Corte, L., Chaikin, P. M., Gollub, J. P. & Pine, D. J. Random organization in periodically driven systems. *Nat. Phys.* **4**, 420–424 (2008).
- Fruchart, M., Hanai, R., Littlewood, P. B. & Vitelli, V. Non-reciprocal phase transitions. *Nature* **592**, 363 (2021).
- Yaron, U. et al. Structural evidence for a two-step process in the depinning of the superconducting flux-line lattice. *Nature* **376**, 753–755 (1995).
- Hellerqvist, M. C., Ephron, D., White, W. R., Beasley, M. R. & Kapitulnik, A. Vortex dynamics in two-dimensional amorphous Mo<sub>77</sub>Ge<sub>23</sub> films. *Phys. Rev. Lett.* **76**, 4022–4025 (1996).
- Moon, K., Scalettar, R. T. & Zimányi, G. Dynamical phases of driven vortex systems. *Phys. Rev. Lett.* **77**, 2778–2781 (1996).
- Ryu, S., Hellerqvist, M., Doniach, S., Kapitulnik, A. & Stroud, D. Dynamical phase transition in a driven disordered vortex lattice. *Phys. Rev. Lett.* **77**, 5114–5117 (1996).
- Balents, L., Marchetti, M. C. & Radzihovsky, L. Nonequilibrium steady states of driven periodic media. *Phys. Rev. B* **57**, 7705–7739 (1998).
- Le Doussal, P. & Giamarchi, T. Moving glass theory of driven lattices with disorder. *Phys. Rev. B* **57**, 11356–11403 (1998).
- Pardo, F., de la Cruz, F., Gammel, P. L., Bucher, E. & Bishop, D. J. Observation of smectic and moving-Bragg-glass phases in flowing vortex lattices. *Nature* **396**, 348–350 (1998).
- Olson, C. J., Reichhardt, C. & Nori, F. Nonequilibrium dynamic phase diagram for vortex lattices. *Phys. Rev. Lett.* **81**, 3757–3760 (1998).
- Kolton, A. B., Domínguez, D. & Grønbech-Jensen, N. Hall noise and transverse freezing in driven vortex lattices. *Phys. Rev. Lett.* **83**, 3061–3064 (1999).
- Troyanovski, A. M., Aarts, J. & Kes, P. H. Collective and plastic vortex motion in superconductors at high flux densities. *Nature* **399**, 665–668 (1999).
- Xiao, Z. L., Andrei, E. Y., Shuk, P. & Greenblatt, M. Equilibration and dynamic phase transitions of a driven vortex lattice. *Phys. Rev. Lett.* **85**, 3265–3268 (2000).
- Okuma, S., Kashiro, K., Suzuki, Y. & Kokubo, N. Order-disorder transition of vortex matter in a-Mo<sub>77</sub>Ge<sub>1-x</sub> films probed by noise. *Phys. Rev. B* **77**, 212505 (2008).
- Blatter, G., Feigel'man, M. V., Geshkenbein, V. B., Larkin, A. I. & Vinokur, V. M. Vortices in high-temperature superconductors. *Rev. Mod. Phys.* **66**, 1125–1388 (1994).
- Chen, J.-X., Mao, J.-W., Thakur, S., Xu, J.-R. & Liu, F. Dynamical phase of driven colloidal systems with short-range attraction and long-range repulsion. *J. Chem. Phys.* **135**, 094504 (2011).
- Granato, E. et al. Glassy phases and driven response of the phase-field-crystal model with random pinning. *Phys. Rev. E* **84**, 031102 (2011).
- Tierno, P. Depinning and collective dynamics of magnetically driven colloidal monolayers. *Phys. Rev. Lett.* **109**, 198304 (2012).
- Reichhardt, C., Olson, C. J., Grønbech-Jensen, N. & Nori, F. Moving Wigner glasses and smectics: dynamics of disordered Wigner crystals. *Phys. Rev. Lett.* **86**, 4354–4357 (2001).
- Danneau, R. et al. Motional ordering of a charge-density wave in the sliding state. *Phys. Rev. Lett.* **89**, 106404 (2002).
- Sengupta, A., Sengupta, S. & Menon, G. I. Driven disordered polymorphic solids: phases and phase transitions, dynamical coexistence and peak effect anomalies. *Phys. Rev. B* **81**, 144521 (2010).
- Reichhardt, C., Reichhardt, C. J. O., Martin, I. & Bishop, A. R. Dynamical ordering of driven stripe phases in quenched disorder. *Phys. Rev. Lett.* **90**, 026401 (2003).
- Zhou, C., Reichhardt, C., Reichhardt, C. J. O. & Beyerlein, I. J. Dynamic phases, pinning, and pattern formation for driven dislocation assemblies. *Sci. Rep.* **5**, 8000 (2015).

51. Reichhardt, C., Ray, D. & Reichhardt, C. J. O. Collective transport properties of driven skyrmions with random disorder. *Phys. Rev. Lett.* **114**, 217202 (2015).
52. Reichhardt, C. & Olson, C. J. Colloidal dynamics on disordered substrates. *Phys. Rev. Lett.* **89**, 078301 (2002).
53. Pertsinidis, A. & Ling, X. S. Statics and dynamics of 2D colloidal crystals in a random pinning potential. *Phys. Rev. Lett.* **100**, 028303 (2008).
54. Deuschländer, S., Horn, T., Löwen, H., Maret, G. & Keim, P. Two-dimensional melting under quenched disorder. *Phys. Rev. Lett.* **111**, 098301 (2013).
55. Macauley, G. M., Paterson, G. W., Macedo, R., McVitie, S. & Stamps, R. L. Tuning magnetic order with geometry: thermalization and defects in two-dimensional artificial spin ices. *Phys. Rev. B* **101**, 144403 (2020).
56. del Campo, A. Universal statistics of topological defects formed in a quantum phase transition. *Phys. Rev. Lett.* **121**, 200601 (2018).
57. Biroli, G., Cugliandolo, L. F. & Sicilia, A. Kibble-Zurek mechanism and infinitely slow annealing through critical points. *Phys. Rev. E* **81**, 050101 (2010).

### Acknowledgements

We thank W. H. Zurek for his useful discussions. We gratefully acknowledge the support of the U.S. Department of Energy through the LANL/LDRD program for this work. This work was supported by the U.S. Department of Energy through the Los Alamos National Laboratory. Los Alamos National Laboratory is operated by Triad National Security, LLC, for the National Nuclear Security Administration of the U.S. Department of Energy (Contract No. 892333218NCA000001).

### Author contributions

CJOR and CR conceived and led the development of the project, performing the numerical analysis. CJOR, AdC, and CR participated in the analysis of the results and the writing of the manuscript.

### Competing interests

The authors declare no competing interests.

### Additional information

**Correspondence** and requests for materials should be addressed to C. J. O. Reichhardt.

**Peer review information** *Communications Physics* thanks the anonymous reviewers for their contribution to the peer review of this work.

**Reprints and permission information** is available at <http://www.nature.com/reprints>

**Publisher's note** Springer Nature remains neutral with regard to jurisdictional claims in published maps and institutional affiliations.



**Open Access** This article is licensed under a Creative Commons Attribution 4.0 International License, which permits use, sharing, adaptation, distribution and reproduction in any medium or format, as long as you give appropriate credit to the original author(s) and the source, provide a link to the Creative Commons license, and indicate if changes were made. The images or other third party material in this article are included in the article's Creative Commons license, unless indicated otherwise in a credit line to the material. If material is not included in the article's Creative Commons license and your intended use is not permitted by statutory regulation or exceeds the permitted use, you will need to obtain permission directly from the copyright holder. To view a copy of this license, visit <http://creativecommons.org/licenses/by/4.0/>.

© The Author(s) 2022